Preferred citation: Z. Shen, K. Oh, M. Toivakka and H.K. Lee. Preparation of cellulose nanofibrils/salt hydrate composite phase change materials for thermal energy storage. In *Advances in Pulp and Paper Research*, Cambridge 2022, Trans. of the XVIIth Fund. Res. Symp. Cambridge, 2022 (D. Coffin and W. Batchelor, eds), pp 157–186. FRC, Manchester, 2022. DOI: 10.15376/frc.2022.1.157.

PREPARATION OF CELLULOSE NANOFIBRILS/SALT HYDRATE COMPOSITE PHASE CHANGE MATERIALS FOR THERMAL ENERGY STORAGE

Zhenghui Shen[1,2], Kyudeok Oh[3,4], Martti Toivakka[4], Hak Lae Lee[2,3]*

[1] Beijing Key Laboratory for Theory and Technology of Advanced Battery Materials, School of Materials Science and Engineering, Peking University, Beijing 100871, China
[2] Department of Agriculture, Forestry and Bioresources, College of Agriculture and Life Sciences, Seoul National University, Seoul 08826, Korea
[3] Research Institute of Agriculture and Life Sciences, Seoul National University, Seoul 08826, Korea
[4] Laboratory of Natural Materials Technology, Åbo Akademi University, Turku 20500, Finland

ABSTRACT

Salt hydrate phase change materials (PCMs) have been intensively used for thermal energy storage (TES) due to their sharp melting points, high energy storage density, small volume change and low cost. However, the problems of phase separation, supercooling and relatively low thermal conductivity of salt hydrate PCMs need to be addressed for high-efficiency TES. In this research, cellulose nanofibrils (CNFs) and CNFs-based composites were used to improve the TES performance of sodium acetate trihydrate (SAT). The effect of

* Corresponding author

CNFs on the phase stability of SAT was investigated and the involved mechanism was explored by the rheological study. CNFs/graphene nanoplatelets (GNPs) composites and CNFs/silver nanoparticles (AgNPs) composites were prepared and used to improve the TES efficiency of SAT. Results indicate that adding 0.8% of CNFs to SAT increased the viscosity, enhanced solid-like rheological behaviors by entangled nanofiber network, and successfully eliminated phase separation of SAT. Owing to the excellent dispersing capability of CNFs, the aggregations of GNPs and AgNPs were avoided in the prepared CNFs/GNPs and CNFs/AgNPs composites. The resulting SAT-based composite PCMs were phase-stable and exhibited improved thermal conductivities over pure SAT due to the thermal conductivity enhancers, GNPs and AgNPs. Besides, with the combined use of sodium phosphate dibasic dodecahydrate and CNFs/$AgNPs_{0.02}$ composite, the supercooling degree of SAT decreased to 1.2 °C. The prepared composite PCMs exhibited reasonable phase change temperature and enthalpy, and improved thermal stability. In summary, green and versatile CNFs-based composites were prepared, and they successfully overcame the drawbacks of salt hydrate PCMs for TES applications.

Key words: Thermal energy storage, Salt hydrate phase change materials, Cellulose nanofibrils-based composites, Phase stability, Supercooling, Thermal conductivity

1 INTRODUCTION

Due to their positive contributions to energy saving and pollution relief, thermal energy storage (TES) techniques have gathered intensive attentions in recent decades. Phase change materials (PCMs) are the essential parts of latent heat thermal energy storage (LHTES) systems, where heat can be stored and released through the phase transitions of PCMs. In contrast to sensible heat storage, LHTES has higher energy storage capacity and could maintain temperature at designated levels by using proper PCMs [1]. Salt hydrates is one of the most studied PCM types because of their wide availability, inexpensive price, high volumetric energy storage density, and small temperature swings in their phase transition processes [2]. They have been found in numerous TES applications, such as solar energy storage, peak load shifting of power systems, energy conservation in buildings, domestic space heating, hot water supplying, and industrial waste heat recovery [3,4].

Sodium acetate trihydrate (SAT) is one of the most promising salt hydrate PCMs for TES applications because of its relatively high heat of fusion

and appropriate melting point for actual applications [5]. Nevertheless, SAT application faces the challenge of phase separation, i.e. in the melting process anhydrous salt hydrate settles down to the bottom of PCM containers due to its higher density than water, leading to a gradually decreased thermal storage capacity [6]. Supercooling, which means a liquid does not crystalize when the temperature is below its freezing point and consequently hinders the timely release of stored thermal energy [7], is another drawback of salt hydrate PCMs. The thermal conductivity of salt hydrate PCMs, although relatively higher than that of organic PCMs, is warmly desired to be improved as doing so can accelerate the speed of energy storage [8]. Therefore, the abovementioned barriers of SAT must be overcome for the fabrication of high-performance TES systems.

Cellulose nanofibrils (CNFs), as nano-sized cellulosic materials, not only possess the advantages of abundant availability, biodegradability, renewability, recyclability and the easiness of various chemical modifications but also have high aspect ratio, high surface area and high mechanical strength [9]. Thanks to these fascinating properties, CNFs have great potential to overcome the drawbacks of SAT and to improve the TES performances. Firstly, the excellent thickening effect of CNFs, i.e. CNFs readily form networks at consistency as low as 0.15% [10], can be used to avoid the phase separation. Importantly, the mechanical strength of the entangled CNFs network can be facilely controlled by altering the consistency of CNFs suspension [11]. If with sufficient strength, the entangled nanofibril networks would help to support the salt hydrates and prevent their sedimentation during melting. Besides, adding CNFs to salt hydrate solutions can increase the viscosity, thus decreasing the flowability of the dispersion. These two effects are expected to solve the problem of phase separation.

Metal nanoparticles (MNPs) serve as typical nucleating agents for decreasing the supercooling degree of salt hydrate. However, these tiny particles aggregate easily due to their large surface areas. The high surface area, thermal stability and tunable surface chemistry of nanocellulose make it good support and stabilizer for nanoparticles [12]. The synthesis and use of CNFs/MNPs composite enables not only the uniform distribution of nucleating nanoparticles for effective supercooling suppression but also the enhancement of thermal conductivity of PCM due to the excellent thermal properties of metal. As a universal thermal conductivity enhancer, carbon nanomaterials (CNMs) are generally introduced to PCMs for boosting their thermal conductivity. Nevertheless, these nanomaterials also suffer from easy aggregation due to the strong van der Waals force between the particles. Interestingly, CNFs exhibit both hydrophilicity by the hydroxyl groups on their surfaces and hydrophobicity by their carbon backbones and this amphiphilicity is capable of dispersing CNMs without harming their intrinsic thermal properties [13]. Therefore, CNFs/CNMs composites are attractive for improving the heat transfer performance of PCMs.

Herein, we report the preparation of CNFs/graphene nanoplatelets (GNPs) and CNFs/silver nanoparticles (AgNPs) composites and their application in SAT for improving the TES performance. First, the morphologies of the prepared CNFs-based composites and the dispersion of nanoparticles (i.e. GNPs and AgNPs) were investigated. Then, their effect on the structures, phase change performance and thermal properties of the prepared composite PCMs were throughly studied. It is expected that this research could give some inspiration on incorporating cellulose-based composites into some important fields, e.g. TES.

2 MATERIALS AND METHODS

2.1 Materials

Bleached eucalyptus kraft pulp (Figure 1(a)) was used to prepare CNFs. Anhydrous sodium acetate (SA, CH_3COONa), sodium tetraborate decahydrate (Borax, $B_4Na_2O_7{\cdot}10H_2O$), sodium phosphate tribasic dodecahydrate ($Na_3PO_4{\cdot}12H_2O$), sodium phosphate dibasic dodecahydrate (DSP, $Na_2HPO_4{\cdot}12H_2O$), and tetrasodium pyrophosphate decahydrate ($Na_4P_2O_7{\cdot}10H_2O$), silver nitrate ($AgNO_3$, purity >99.0%), sodium borohydride ($NaBH_4$, purity >99.0%), nitric acid (HNO_3), and GNPs (surface area 500 m^2/g) were all purchased from Sigma-Aldrich (St Louis, MO, USA). These materials were used as received without further purification or modification, and deionized water was used in all experiments.

2.2 Preparation of CNFs and CNFs-Based Composites

CNFs were prepared by grinding a 2 wt% pulp suspension through a grinder (Super Masscolloider, Masuko Sangyo Co., Ltd., Kawaguchi-city, Japan) for 30 times. The gap between the two grinding plates was -80 μm, and the grinding speed was 1500 rpm. The zeta potential of the prepared CNFs (Figure 1(b)), examined with a Malvern Zetasizer (Nano-ZS, Malvern Instruments Ltd., Worcestershire, UK) was -34.8 ± 0.5 mV. The charge density determined by a titration method was 0.16 meq/g CNFs.

CNFs/GNPs composites were prepared by homogenizing GNPs in a 0.5 wt% CNFs suspension for 60 min using an Ultra-Turrax T50 homogenizer (Janke & Kunkel, IKA-Labortechnik, Staufen, Germany), followed by centrifugation (Combi R514, Hanil Scientific Inc., Gimpo, Korea) at 9000 rpm for 30 min. To prevent over heating of the samples, an ice bath was used and a 2-min pause was adopted after each 10-min homogenization. Different mass ratios between CNFs and GNPs (0.8:0.5, 0.8:1.5, and 0.8:2.5) were used to obtain a series of

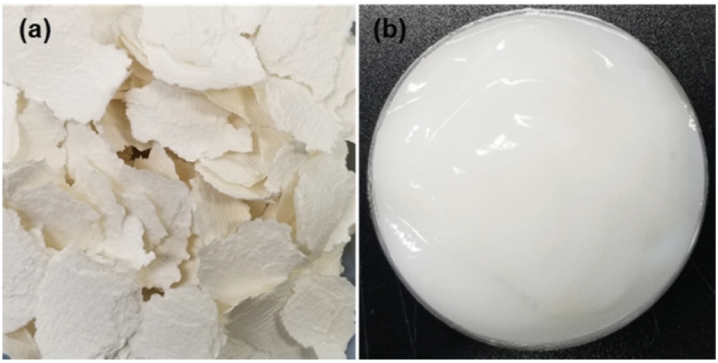

Figure 1. Digital image of (a) commercial bleached eucalyptus kraft pulp and (b) the prepared CNFs.

composites, which were labelled as CNFs/$GNPs_{0.5}$, CNFs/$GNPs_{1.5}$, and CNFs/$GNPs_{2.5}$, where the subscripts indicate the dose (%) of the GNPs.

CNFs/AgNPs composites were synthesized using the chemical reduction reaction between $AgNO_3$ and $NaBH_4$ performed in CNFs suspensions. Specifically, prepared CNFs suspension (0.5 wt%, 100 g) was mixed with a 0.01 M $AgNO_3$ solution (100 mL), followed by mechanical mixing of the resulting CNFs/$AgNO_3$ mixture at room temperature for 30 min in darkness and then an ice incubation for 20 min. 0.1 M $NaBH_4$ solution (200 mL) was prepared and incubated in an ice bath under mixing for 20 min. The CNFs/$AgNO_3$ mixture was then added drop-by-drop to the $NaBH_4$ solution while mixing, and the reaction was allowed to occur for another 20 min. The reaction mechanism is shown by Eq. (1):

$$AgNO_3 + NaBH_4 \rightarrow Ag + NaNO_3 + 1/2\ H_2 + 1/2\ B_2H_6 \quad (1)$$

The concentration of $NaBH_4$ solution was fixed while $AgNO_3$ solutions of varied concentrations (0.01M, 0.02M and 0.03M) were used to prepare CNFs/AgNPs composites with different silver contents. The synthesized composites were also collected by centrifugation operations and were denoted as CNFs/$AgNPs_{0.01}$, CNFs/$AgNPs_{0.02}$ and CNFs/$AgNPs_{0.03}$, with the subscript indicating $AgNO_3$ concentration used for synthesis. The silver content of the synthesized CNFs/AgNPs composites was determined by a liquid chromatography-inductively coupled plasma mass spectrometer (ICP-MS, JP/7900, Agilent technologies, Santa Clara, CA, USA). Prior to analysis, the composite suspension (1 mg/mL) was digested using concentrated HNO_3 in a microwave sample digestion system (MARS-6, CEM Corp., Matthews, NC, USA) for 30 min.

SAT-based composite PCMs were fabricated by sequentially dispersing CNFs or CNFs-based composites, DSP, and SA while mixing in deionized water, and the SA:H_2O molar ratio was set to 1:3. Then the obtained mixture was magnetically mixed for 1.5 h in a 70 °C water bath for complete melting of salt hydrate and better uniformity of composite PCMs. Depending on the used CNFs-based composites, GNPs containing composite PCM were labelled as PCM@CNFs/$GNPs_{0.5}$, PCM@CNFs/$GNPs_{1.5}$ and PCM@CNFs/$GNPs_{2.5}$, and AgNPs containing composite PCMs were named as PCM@CNFs/$AgNPs_{0.01}$, PCM@CNFs/$AgNPs_{0.02}$ and PCM@CNFs/$AgNPs_{0.03}$. Analogously, composite PCM containing pristine CNFs was prepared and was denoted as PCM@CNFs. Solid PCM samples were obtained by the spontaneous crystallization of liquid dispersions at room temperature, i.e. a temperature lower than the freezing point of the dispersion samples. Then solid blocks or pieces of the solidified samples were used for scanning electron microscopy (SEM), differential scanning calorimetry (DSC) and thermogravimetric (TG) analyses, and solid powders were prepared and used for Fourier transform-infrared spectra (FT-IR), X-ray diffraction (XRD) and thermal conductivity analyses.

2.3 Characterizations

2.3.1 Phase Stability and Rheology Tests

To perform the phase stability test, 18 g of samples were placed in glass tubes with lids, followed by a 2-h incubation in a 70 °C water bath. Then these tubes were removed, and phase stability was observed and recorded with digital images. The fluidity of samples was determined by inverting the bottles and noting their flowability. Rheological properties of samples like viscosity, storage (G') and loss (G'') moduli were investigated at 65 °C using a stress-controlled rotational rheometer (CVO-100-901, Malvern Instruments Ltd., Worcestershire, UK) with a cone-plate geometry (R=40 mm, angle=4°). To minimize the moisture loss of samples, a cover was used to seal them inside and water droplets were uniformly spread around the samples.

2.3.2 Determination of Supercooling Degree

The supercooling degrees of SAT and SAT-based composite PCMs were determined by a T-history method [14] and the experimental setup is schematically shown in Figure 2. In brief, 10 g of PCM sample was put in the test tube with a lid and was then incubated in a hot water bath at 70 °C for 1 h, followed by natural cooling in air. The real-time temperature in cooling was obtained by a thermocouple (PT100, Pico Technology Ltd., Cambridgeshire, UK), and was

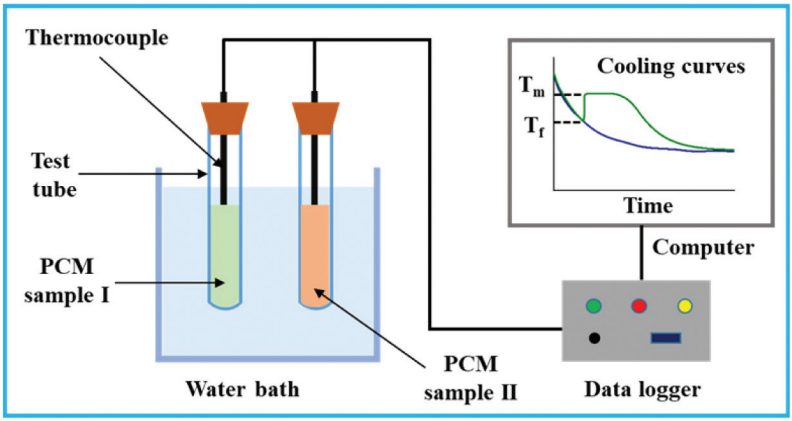

Figure 2. Experimental setup for the measurement of supercooling degree of PCM.

collected by temperature data logger (PT-104, Pico Technology Ltd., Cambridgeshire, UK). The supercooling degree of PCM was calculated according to Eq. (2):

$$\Delta T_S = T_m - T_f \tag{2}$$

where ΔT_s means the supercooling degree of PCM (°C), T_m is the melting point of PCM (°C), and T_f denotes the freezing point of PCM (°C).

2.3.3 Transmission Electron Microscopy Analysis

The morphologies of CNFs, GNPs and CNFs-based composites were recorded with an energy-filtering transmission electron microscope (TEM, LIBRA 120, Carl Zeiss, Oberkochen, Germany). Samples with a concentration of 0.002% were prepared and deposited on the copper grid (Ted Pella, Inc., Redding, CA, USA), followed by drying at room temperature. For a clear observation, CNFs containing samples were negatively stained with a 2% uranyl acetate (UA) solution for 30 s before the analysis. In particular, the particle size of AgNPs was calculated using ImageJ software (ImageJ 1.53a, National Institutes of Health, USA). The average particle size and particle size distribution of AgNPs were obtained by counting more than 300 nanoparticles in each CNFs/AgNPs composite.

2.3.4 Scanning Electron Microscopy Analysis

The structures of the SAT and SAT-based composite PCMs were recorded with field-emission scanning electron microscopy (FE-SEM, Auriga, Carl Zeiss,

Oberkochen, Germany) under a vacuum with an acceleration voltage of 2 kV. Before the analysis, samples were sputtered with platinum in an argon atmosphere at 30 mA for 150 s.

2.3.5 UV-Visible Spectroscopy

Ultraviolet-visible (UV/Vis) spectroscopy analysis was carried out using an Optizen Alpha UV/Vis spectrophotometer (K Lab Co., Ltd., Daejeon, Korea) in 200–700 nm wavelength range. To confirm the successful synthesis of AgNPs, CNFs or CNFs/AgNPs composites were dispersed into deionized water to obtain samples with 0.01% concentration and injected to quartz cuvettes for the tests. To show its stability in the presence of sodium salt, $CNFs/AgNPs_{0.02}$ composite was dispersed in same amounts of deionized water and sodium acetate solution with different concentrations (i.e. 0.2 N and 1 N), and the UV/Vis spectra were recorded and compared.

2.3.6 Fourier Transform-Infrared Spectra

Fourier transform-infrared (FT-IR) spectra of samples were obtained by a Nicolet 6700 spectrometer equipped with an attenuated total reflection (ATR) accessory (Thermo Scientific, Waltham, MA, USA). The analysis was performed in the range of 650–4000 cm^{-1} at a resolution of 2 cm^{-1}.

2.3.7 X-ray Diffraction Analysis

X-ray diffraction (XRD) patterns of samples were collected using a Bruker diffractometer (D8 Advance, Bruker AXS GmbH, Karlsruhe, Germany) with Cu Kα1 radiation at $\lambda = 1.5418$ Å operating at 40 kV and 40 mA. The analysis was performed with a scanning speed of 2.4°/min.

2.3.8 Differential Scanning Calorimetry Analysis

The phase change properties of PCMs, including melting point and enthalpy were investigated using differential scanning calorimetry (DSC, Discovery DSC, TA Instruments Inc., New Castle, DE, USA). Samples were heated from 25 °C to 70 °C at a rate of 5 °C/min under a 20 mL/min nitrogen purge.

2.3.9 Thermogravimetric Analysis

The thermal stability of PCMs was examined using a thermogravimetric analyzer (TGA, TGA4000, PerkinElmer Inc., Waltham, MA, USA). Samples were heated from 30 °C to 200 °C at 5 °C/min with a nitrogen flow rate of 20 mL/min.

2.3.10 Thermal Conductivity Measurements

Powdered sample was pressed into pellet (10 mm in diameter, approximately 2 mm in thickness) under a pressure of 100 kg/cm^2 for 10 min. The mass and thickness of the prepared pellet were measured, and the density was calculated. The thermal diffusivity of PCM pellet was measured by a laser flash apparatus (LFA467, Netzsch Instruments, Selb, Germany). The thermal conductivity k (W/(m·K)) was then calculated according to Eq. (3):

$$k = \alpha \cdot C_P \cdot \rho \tag{3}$$

where α is thermal diffusivity of PCM pellet (mm^2/s), C_P presents specific heat (J/(kg·K)), and ρ means the density of pellet (kg/m^3).

2.3.11 Thermal Reliability Measurements

The thermal reliability of the PCM samples was studied by comparing their chemical stability and phase change properties (melting point and enthalpy) before and after 100 melting/freezing cycles.

3 RESULTS AND DISCUSSION

3.1 Effect of CNFs on Phase Stability of PCMs

Phase separation occurs due to the difference of densities of salt hydrate and water in the melting process, and this can be addressed by adding thickening agents such as polyacrylic amide, poly (acrylamide-*co*-acrylic acid) partial sodium salt, sodium polyacrylate, and polyvinyl alcohol [15–18]. These materials are soluble in aqueous phase, and increase the viscosity of salt hydrate solution so that flowing or precipitation of salt hydrate is hindered. However, most of them are synthesized and have negative environmental impacts. Carboxymethyl cellulose (CMC), a type of cellulose derivative, has been widely used to avoid the phase separation of salt hydrate PCMs. For example, Liu *et al.* incorporated CMC as the thickening agent into SAT for fabricating a composite PCM [17]. When 3% of CMC was applied, the phase separation of SAT was prevented, suggesting its effectiveness in thickening the salt hydrate solutions.

The excellent gelling performance of CNFs and their compatibility with salt hydrate make them a promising candidate for resolving the phase separation of SAT. In research by Oh *et al.*, the effects of CMC and CNFs on stabilizing sodium sulfate decahydrate (SSD) and the mechanism therein were investigated [19]. For comparison, cellulose microfibrils (CMFs), unmodified CNFs and TEMPO-oxidized CNFs were prepared and used in their research. The phase stability

observations suggest that chemically modified CNFs with high charge density failed to prevent the phase separation of SSD because the nanofibrils network structure was destroyed by the high ionic concentration of dissolved salt. In contrast, both CMFs and CNFs successfully avoided the phase separation of SSD as their entangled networks were not damaged by salt dissolution, and CNFs gave a greater stabilizing effect due to their higher surface area that induced stronger entangling capability than CMFs. The viscoelastic properties of PCM slurries with/without cellulosic thickening agents were measured, and it was shown that pristine CNFs exhibited the most promising stabilizing effect for SSD. The results also verify that CMC did not function as effectively as CNFs, even when its dosage was higher. The reason was CMC stabilized the salt hydrate by increasing the slurry viscosity after its dissolution, but there was a lack of entangled network that can prevent the precipitation of anhydrous salt. This study demonstrates the feasibility of utilizing sustainable CNFs rather than synthetic polymers to solve the phase separation issue of salt hydrate PCMs. Hence, CNFs without any chemical modification were used in this work to cope with the phase separation of SAT, considering their advantages in providing a stronger entangled network in salt solution.

Figure 3(a) shows the effect of CNFs dosage on the phase stability of SAT. Typical phase separation of SAT is visible without addition of CNFs. However, less free water appeared in the upper part of samples with the increase of CNFs addition. When 0.8% of CNFs was added, the phase stability of SAT was realized and the phase separation problem was successfully addressed. The fluidity test result (Figure 3(b)) indicates that the flowability of samples decreased with the incorporation of CNFs into SAT. When the CNFs dosage was higher than 0.6%, the gel-like structure of samples was maintained and samples did not flow downward. This implies that the viscosity of samples became higher with the addition of CNFs. Because of the entangled CNFs networks and the increased viscosity, phase separation was avoided, which are interpreted via rheological studies. The viscosity results (Figure 3(c)) suggest that all the samples exhibited shear-thinning behavior, as suggested by the power law index $n<1$. A shoulder-like stage appeared in the curves, especially when CNFs content was higher than 0.4%. This can be attributed to the disruption of the entangled CNFs networks needed stronger stress, thus the viscosity increased accordingly. Afterward, the rearrangement of CNFs networks was completed, leading to a continuous decrease in viscosity.

The yield stress of samples, i.e. the point where G' drops suddenly and meets G", can be used to evaluate the strength of the formed CNFs networks in samples. As shown by the amplitude sweep results (Figure 3(d)), the yield stress increased with the increased CNFs content up to 0.8%, after which no more increase can be seen. This indicates that 0.8% of CNFs was sufficient to provide the strongest network in SAT, which agrees with the result of the phase stability test. The frequency sweep results (Figure 3(e)) demonstrate that G' was much higher than

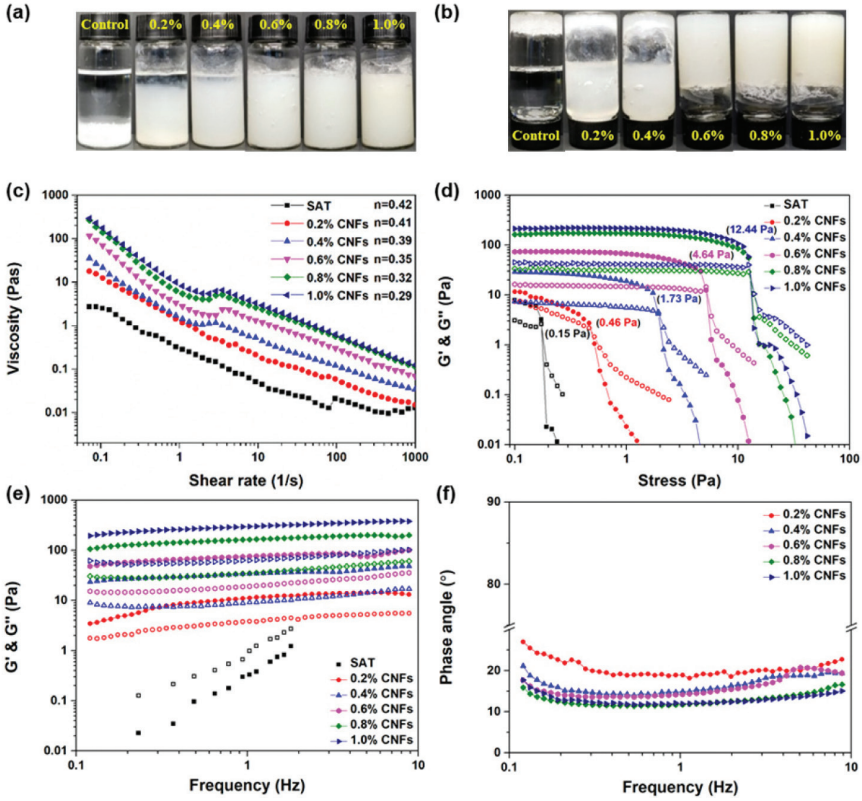

Figure 3. (a) Phase stability test, (b) fluidity test, (c) viscosity as a function of shear rate and (d) amplitude sweep test of SAT/CNFs mixtures with varied CNFs contents, (e) frequency sweep test of SAT/CNFs mixtures with varied CNFs contents, and (f) phase angle of samples in the frequency sweep test. Closed symbols in (d) and (e): storage modulus (G'); open symbols in (d) and (e): loss modulus (G").

G″ over the entire testing range of 0.1–10 Hz, which suggests a more solid-like rheology behavior of CNFs containing samples. However, SAT solution displays a liquid-like rheology behavior, as evidenced by a G″ that was higher than G'. The dominating elastic portion in the viscoelasticity of the CNFs containing samples was verified by the fact that all of the samples had phase angles less than 45° (Figure 3(f)) that indicates a more solid-like rheology behavior [20]. These results prove that adding CNFs to SAT introduced 3D entangled nanofibrils networks, increased the viscosity, and improved the solid-like rheology performance of salt hydrate, consequently eliminating phase separation of SAT.

When CNFs/GNPs was added to SAT, stable phase was also obtained (Figure 4(a)), indicating that the presence of GNPs did not negate the thickening effect of CNFs. As expected, when only GNPs were added to SAT phase separation occurred, and both GNPs and anhydrous salt settled down. This occurred due to the facts that GNPs themself do not have the network forming ability and they

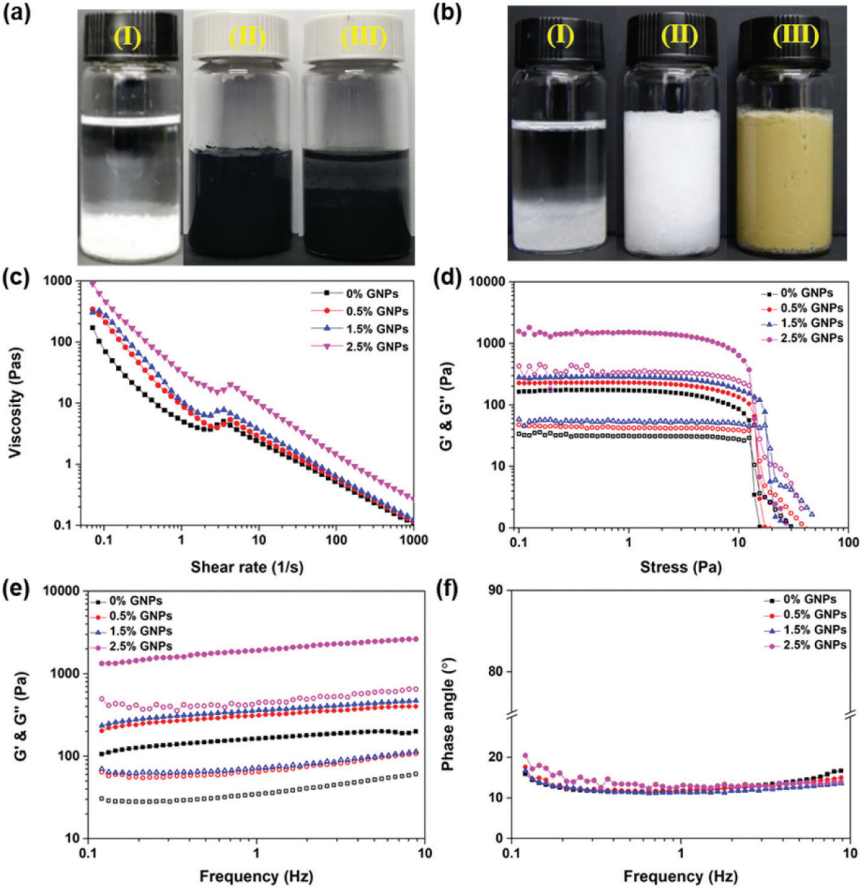

Figure 4. (a) Phase stability test of (I) pure SAT, (II) PCM sample with CNFs/GNPs$_{2.5}$ composite and (III) PCM sample with 2.5% GNPs, and (b) phase stability test of (I) pure SAT, (II) PCM sample with CNFs, and (III) PCM sample with CNFs/AgNPs$_{0.02}$ composite; rheological tests of SAT/CNFs/GNPs composites with varied GNPs contents: (c) viscosity depending on shear rate, (d) amplitude sweep test, (e) frequency sweep test and (f) phase angle in frequency sweep test. Closed symbols in (d) and (e): storage modulus (G'); open symbols in (d) and (e): loss modulus (G'').

have a higher density than water. The effect of adding GNPs on the rheological properties of PCM samples was investigated. The viscosity results (Figure 4(c)) indicate that adding GNPs increased the viscosity of samples due to the closer contact and more interactions between the solid components. The shoulder-like regions still existed on the viscosity-shear rate plots, which was ascribed to the structure change of CNFs networks under the varied shearing. Both amplitude sweep (Figure 4(d)) and frequency sweep (Figure 4(e)) results show that increasing the addition levels of GNPs resulted in higher G' and G", which indicates enhanced solid-like behavior of samples. Interestingly, the yield points (Figure 4(d)) of these samples remained unchanged with increased GNPs addition, suggesting that CNFs rather than GNPs contributed to the strength of the entangled networks. The phase angles (Figure 4(f)) of GNPs containing PCM samples were quite similar to each other, confirming the CNFs play the dominating role in providing the solid-like behavior of the samples. The effect of CNFs/AgNPs addition on phase stability was also explored. As shown in Figure 4(b), phase separation was resolved by adding either CNFs or CNFs/AgNPs composite. CNFs have strong network forming capability and this was not obviously affected by AgNPs. The above analyses verify that the prepared PCM composites containing CNFs or CNFs-based composite were phase-stable, which will allow salt hydrate PCMs to contribute more efficiently to the TES process.

3.2 Morphologies of CNFs/GNPs and CNFs/AgNPs Composites

CNFs/GNPs composites were prepared by homogenizing GNPs in CNFs suspensions, and the digital image of the prepared CNFs/GNPs$_{2.5}$ composite is shown in Figure 5(a). The composite has a gel-like appearance similar to that of CNFs, and it is black due to the introduction of GNPs. The TEM image (Figure 5(b)) of the purchased GNPs shows that several layers of graphene stacked together, which can be ascribed to the strong van der Waals force between the adjacent layers. Figure 5(c) presents the typical morphology of CNFs, i.e. high aspect ratio and entangled network structure. When 0.5% of GNPs was used to prepare the composite, sufficient amount (0.8%) of CNFs enables the good exfoliation and dispersion of the GNPs, and single layered GNPs are visible (Figure 5(d)). When 1.5% of GNPs was used, multilayered GNPs can be seen in Figure 5(e). When 2.5% of GNPs was added, the CNFs/GNPs suspension was too thick to have a uniform dispersion of GNPs, and both single layered GNPs and multilayered GNPs can be found in Figure 5(f). Therefore, it is important to consider the ratio between CNFs and carbon nanomaterials and the suspension consistency when dispersing nanocarbon using CNFs. The prepared CNFs/GNPs composites were then blended with other components to prepare composite PCMs.

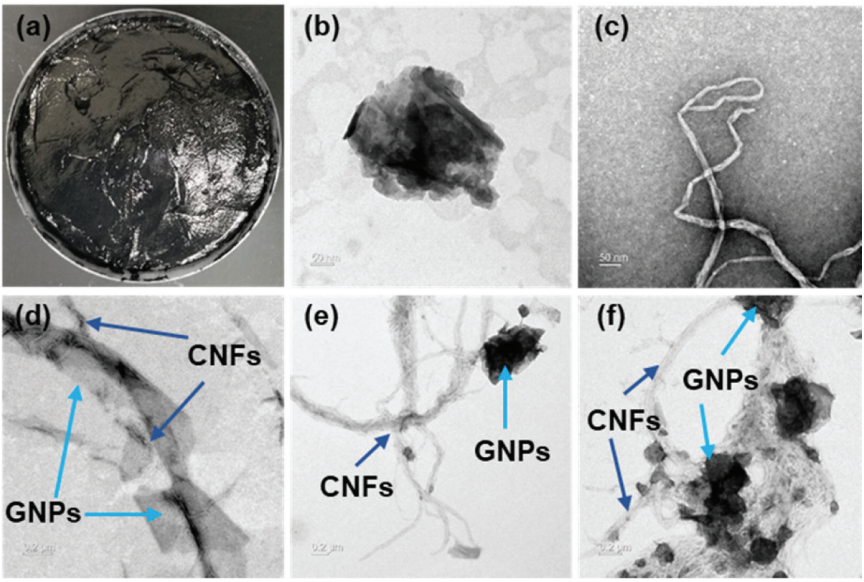

Figure 5. Digital image of the prepared CNFs/$GNPs_{2.5}$ composite, and TEM images of (b) GNPs, (c) CNFs, (d) CNFs/$GNPs_{0.5}$, (e) CNFs/$GNPs_{1.5}$, and (f) CNFs/$GNPs_{2.5}$ composites.

The formation of AgNPs is comprised of four steps, including (i) rapid reduction of silver ions by $NaBH_4$, (ii) the reduced silver atoms form clusters until AgNPs have certain stability that stops the process of coalescence, (iii) and (iv) further growth due to coalescence and eventually result in synthesized AgNPs [21]. After these steps, stable AgNPs will be obtained and immobilize on the surface of CNFs, and the CNFs/AgNPs composite is produced. The digital images of the synthesized CNFs/AgNPs composites are presented in Figures 6(a), 6(b) and 6(c). These composites became darker with the increased $AgNO_3$ concentration for AgNPs synthesis. The reason is that the reducing agent is excessive, increasing the amount of silver ions in the synthesis led to the increased amount of synthesized AgNPs in the prepared CNFs/AgNPs composites. This was confirmed by the ICP-MS results (Table 1). Figures 6(d), 6(e) and 6(f) show the morphologies of the synthesized CNFs/AgNPs composites. Successful synthesis of AgNPs was confirmed, and these nanoparticles are well dispersed and stabilized by CNFs. No obvious aggregations of nanoparticles were noted in these TEM images. The average particles size and its distribution of AgNPs are presented in Figures 6(g), 6(h) and 6(i). It was found that when increasing the

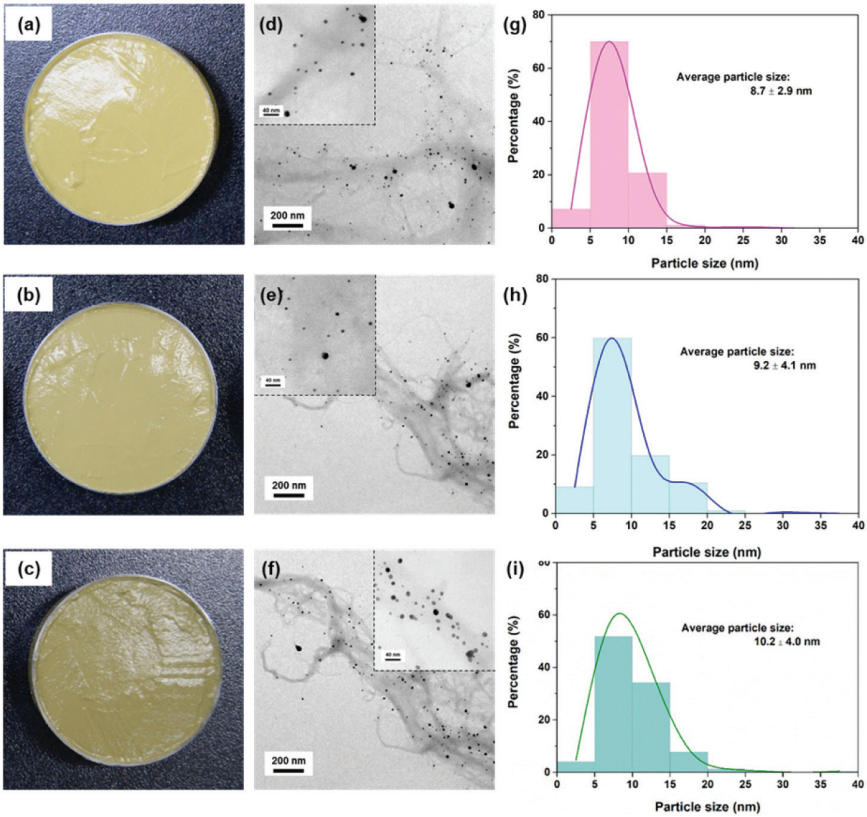

Figure 6. Digital images of the synthesized CNFs/AgNPs composites: (a) CNFs/$AgNPs_{0.01}$, (b) CNFs/$AgNPs_{0.02}$ and (c) CNFs/$AgNPs_{0.03}$; TEM images of the prepared CNFs/AgNPs composites: (d) CNFs/$AgNPs_{0.01}$, (e) CNFs/$AgNPs_{0.02}$ and (f) CNFs/$AgNPs_{0.03}$, and particle size distribution of the synthesized AgNPs in (g) CNFs/$AgNPs_{0.01}$, (h) CNFs/$AgNPs_{0.02}$ and (i) CNFs/$AgNPs_{0.03}$.

concentration of silver precursor from 0.01 M to 0.03 M, the average particle size of synthesized AgNPs increased accordingly from 8.7 nm to 10.2 nm. Compared to composites CNFs/$AgNPs_{0.01}$ and CNFs/$AgNPs_{0.03}$, CNFs/$AgNPs_{0.02}$ had medium proportions of AgNPs with size in the range of 5–10 nm, while it had higher percentage of AgNPs with size in the range of 15–20 nm. The differences in particle size and its distribution may have an effect on the supercooling suppression of SAT, which was investigated in Section 3.3.

Table 1. Silver content of the synthesized CNFs/AgNPs composites

Composite	*Silver concentration* (mg/kg)	*Silver content* (%)
$CNFs/AgNPs_{0.01}$	77	7.7
$CNFs/AgNPs_{0.02}$	175	17.5
$CNFs/AgNPs_{0.03}$	296	29.6

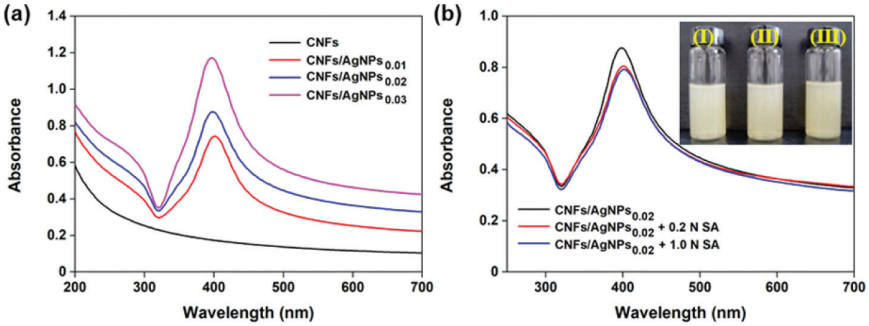

Figure 7. UV/Vis spectra of (a) CNFs and CNFs/AgNPs composites and (b) UV/Vis spectra of $CNFs/AgNPs_{0.02}$ composite (I) and this composite in a 0.2 N (II) and in 1.0 N (III) SA solutions.

Figure 7(a) compares the UV/Vis spectra of CNFs and CNFs/AgNPs composites. No characteristic peak was observed in the spectra of CNFs. However, a single and narrow band centered at 400 nm was found in all spectra of the three CNFs/AgNPs composites, suggesting the successful synthesis and uniform dispersion of AgNPs [22]. The stability of AgNPs in salt solution was investigated by comparing UV/Vis spectra of $CNFs/AgNPs_{0.02}$ composites at different salt concentrations. The characteristic peaks of AgNPs remained unshifted when increasing the salt concentration, which indicates the excellent stability of the prepared CNFs/AgNPs composite in SA solutions. The inset digital image in Figure 7(b) negates the sedimentation or aggregation of AgNPs, addressing the concern of destabilization of AgNPs by salt solution.

3.3 Supercooling Suppression of SAT

The most effective nucleating agent was first selected from four salt hydrate candidates that include $Na_2HPO_4 \cdot 12H_2O$, $Na_4P_2O_7 \cdot 10H_2O$, $B_4Na_2O_7 \cdot 10H_2O$, and $Na_3PO_4 \cdot 12H_2O$. The supercooling degree of SAT affected by each candidate was

determined from the cooling curves (Figure 8). To mimic the real condition, CNFs were added with screening nucleating agent. Without the use of nucleating agent, SAT exhibits a serious supercooling phenomenon and the supercooling degree was as high as over 35 °C. The supercooling of SAT was unaffected upon the addition of CNFs, which is likely attributed to their fibrous morphology that does not trigger the crystallization of SAT. $Na_3PO_4{\cdot}12H_2O$ (Figure 8(a)) and Borax (Figure 8(b)) were ineffective nucleating agents for SAT at all addition levels, although they function in other report [23]. The reason might be that different thickening agents (i.e. CMC and polyacrylamide) were used in the previous study and their combination with nucleating agents must be optimized. $Na_4P_2O_7{\cdot}10H_2O$ (Figure 8(c)) showed positive effect on the supercooling suppression of SAT, and the lowest supercooling degree of 13.6 °C was achieved when its dosage was 1%. DSP was proven to be the most effective nucleating agent for SAT when using CNFs as the thickening agent. When 3% of DSP was applied, the supercooling degree was as low as 2.1 °C, and the crystallization of SAT

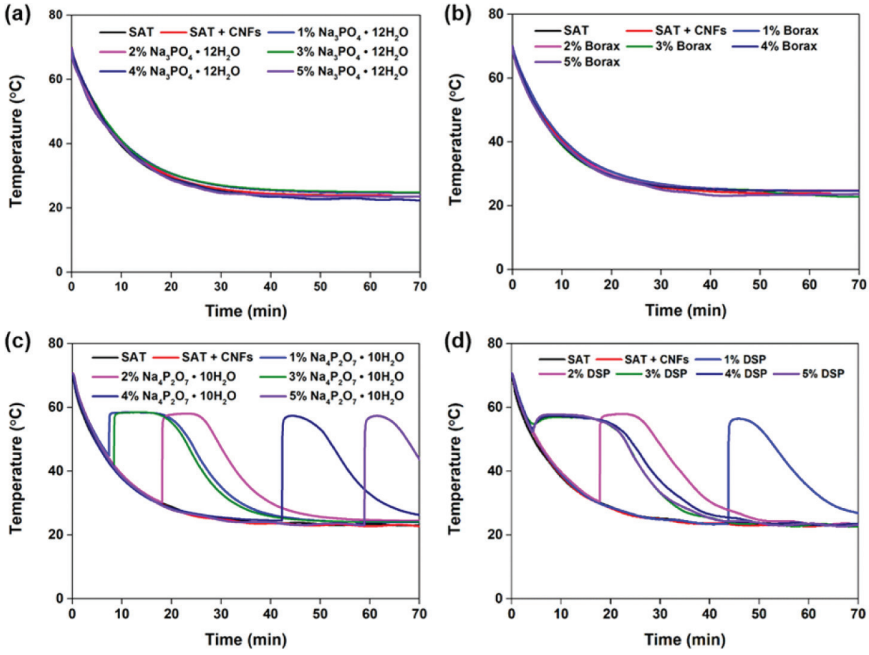

Figure 8. Screening of nucleating agents: (a) $Na_3PO_4{\cdot}12H_2O$, (b) $B_4Na_2O_7{\cdot}10H_2O$ (Borax), (c) $Na_4P_2O_7{\cdot}10H_2O$ and (d) $Na_2HPO_4{\cdot}12H_2O$ (DSP).

occurred shortly (< 5 min) when cooling started. Either a lower or higher dosage than 3% of DSP was added, a slower crystallization and a higher supercooling degree were found. When insufficient nucleating is used, there is a lack of nucleating sites for crystal formation and growth; however, when excessive nucleating agent is applied, the contact area between the nuclei and liquid/substrate increases, thus creating a resistance for nucleation [18]. Hence, DSP was used as the NA for SAT in the follow-up experiments. To summarize, both the combination of thickening agent and NA, and the dosage of NA affect the crystallization behavior of salt hydrate PCMs, which must be considered when selecting appropriate NA.

The effect of adding CNFs/GNPs composites on the supercooling suppression efficiency of DSP was investigated (Figure 9). Compared to samples with only CNFs, GNPs containing PCM samples crystallized rapidly within 5 min as cooling was initiated, and the supercooling degree of SAT was minimally affected. These results indicate that the use of CNFs/GNPs composites does not have obvious negative effect on the supercooling suppression efficiency of nucleating agent DSP. In research by Fashandi and Leung [6], the addition of GNPs increased the supercooling degree regardless of the dosage, and the authors ascribed this to the agglomeration of GNPs, which created porous spaces in the PCM structures and restricted the mobility of SAT molecules and thus impeded the crystallization of SAT. This also indicates that using CNFs as the thickening agent improved the dispersion of GNPs and prevented serious agglomeration, consequently minimally affecting the supercooling suppression efficiency of DSP.

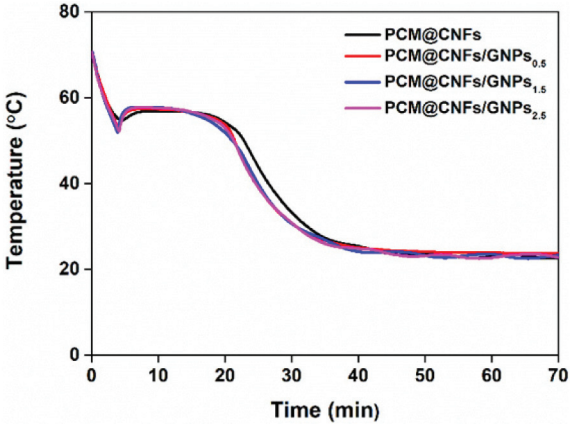

Figure 9. The effect of adding CNFs/GNPs composites on the supercooling suppression of SAT.

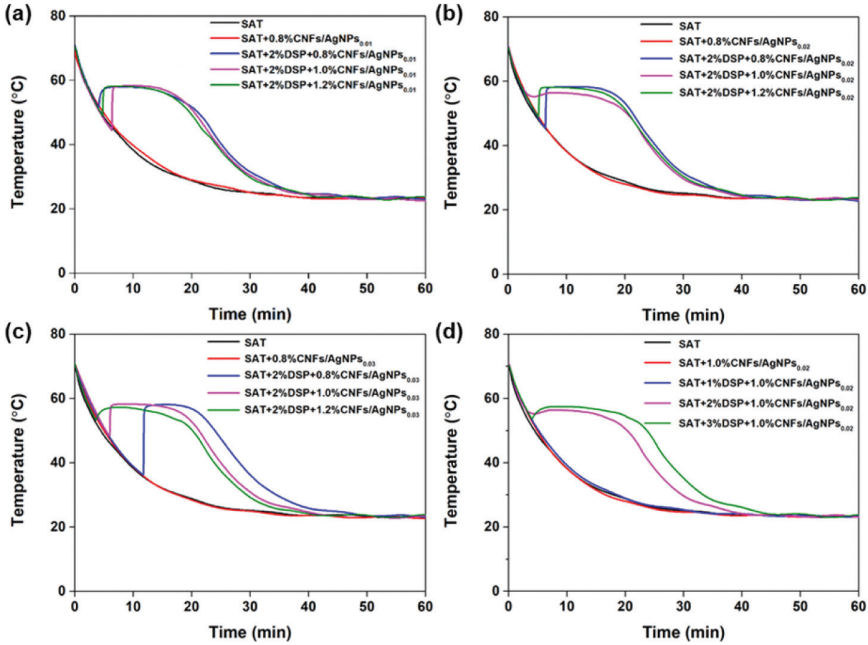

Figure 10. Supercooling suppression of SAT by the combined use of CNFs/AgNPs composites and DSP: effect of (a) CNFs/AgNPs$_{0.01}$, (b) CNFs/AgNPs$_{0.02}$ and (c) CNFs/AgNPs$_{0.03}$ with the dosage of DSP fixed at 2% and (d) effect of DSP with the dosage of CNFs/AgNPs$_{0.02}$ fixed at 1%.

The effect of adding CNFs/AgNPs composites on the supercooling suppression efficiency of DSP was investigated (Figure 10). It was found that the sole addition of these CNFs/AgNPs composites failed to trigger the crystallization process of SAT, and the supercooling of PCM samples occurred for the all these AgNPs containing composite PCMs. However, when CNFs/AgNPs composite was used with DSP, the supercooling of SAT was prohibited. Based on the results of the screening of proper CNFs/AgNPs composite and its suitable dosage (Figures 10(a), 10(b) and 10(c)), 1.0% of CNFs/AgNPs$_{0.02}$ proved to have the greatest capacity in decreasing the supercooling degree of SAT when used with 2% of DSP. This is probably attributed to its medium particle size and the unique particles size distribution. The dosage optimization of DSP (Figure 10(d)) indicates that 2% of DSP was the most suitable dose for its combined use with 1% of CNFs/AgNPs$_{0.02}$ composite. As a result, the crystallization of SAT happened much faster and its supercooling degree was only 1.2 °C, a value that is lower than when 3% of DSP

was added as the sole nucleating agent. Based on these analyses, the combined use of CNFs/AgNPs composite with DSP showed a synergistic effect on facilitating the crystallization of SAT in its cooling process. Generally, two steps account for the crystallization process of SAT: nucleation and crystal growth [24]. In the nucleation step, nucleating sites form to seed crystallization of SAT; in the crystal growth step, SAT crystals start to grow on the surface of NA. When SAT crystallization is initiated, anhydrous SA combines with free water in PCM sample to form salt hydrate, during which latent heat is released. The crystallization of SAT finishes when all the anhydrous salt reunites with water to form hydrated salt. Based on the above cooling tests, DSP was the predominant contributor to the nucleation step and CNFs/AgNPs were more involved in the crystal growth step, in which SAT crystals grow on the surfaces of AgNPs.

3.4 Structures of Composite PCMs

The structures of SAT and SAT-based PCM composites are presented in Figure 11. Figure 11(a) shows that pure SAT has a micron-sized crystal structure and large voids are visible in the structure. When other components (i.e. DSP, CNFs, CNFs/GNPs, CNFs/AgNPs) were incorporated, the structure of composite PCMs became more compact (Figures 6(b–e) and Figure 6(k)) and the SAT crystal size decreased, suggesting good affinity between the components. SEM images with higher magnifications (Figures 11(f–j) and Figure l) were recorded to show the internal structure of composite PCMs and the interactions between the components. Figure 11(f) presents the morphology of a SAT crystal, and some pores are visible on the surface, similar to the finding in Figure 11(a). Figures 11(g–j) and Figure l indicate that CNFs appeared to act as bridges to connect other components. Although a number of GNPs and AgNPs are attached to the surface of CNFs, the abundant hydroxyl groups of CNFs still enable the hydrogen bond of CNFs-based composites with salt hydrates DSP and SAT. When CNFs/$GNPs_{0.5}$ was used to prepare the composite PCM, it is hard to see the graphene nanoparticles (Figure 11(h)), which are clearly observed when CNFs/$GNPs_{1.5}$ (Figure 11(i)) and CNFs/$GNPs_{2.5}$ (Figure 11(j)) composites were used. SAT-wrapped AgNPs (Figure 11(l)) are seen when CNFs/AgNPs composite was used to prepare composite PCM, which also verifies the hypothesis that AgNPs accelerated the crystal growth on their surfaces. Moreover, uniform distribution of AgNPs in the prepared PCM composite (Figure 11(m)) was obtained, which favors the heat conduction in real applications. To sum up, the prepared composite PCMs exhibited compact structure and CNFs-based composites had compatibility with other components.

FT-IR spectra of SAT-based composite PCMs and their components are shown in Figure 12(a) and Figure 12(e). In the spectrum of SAT, the characteristic

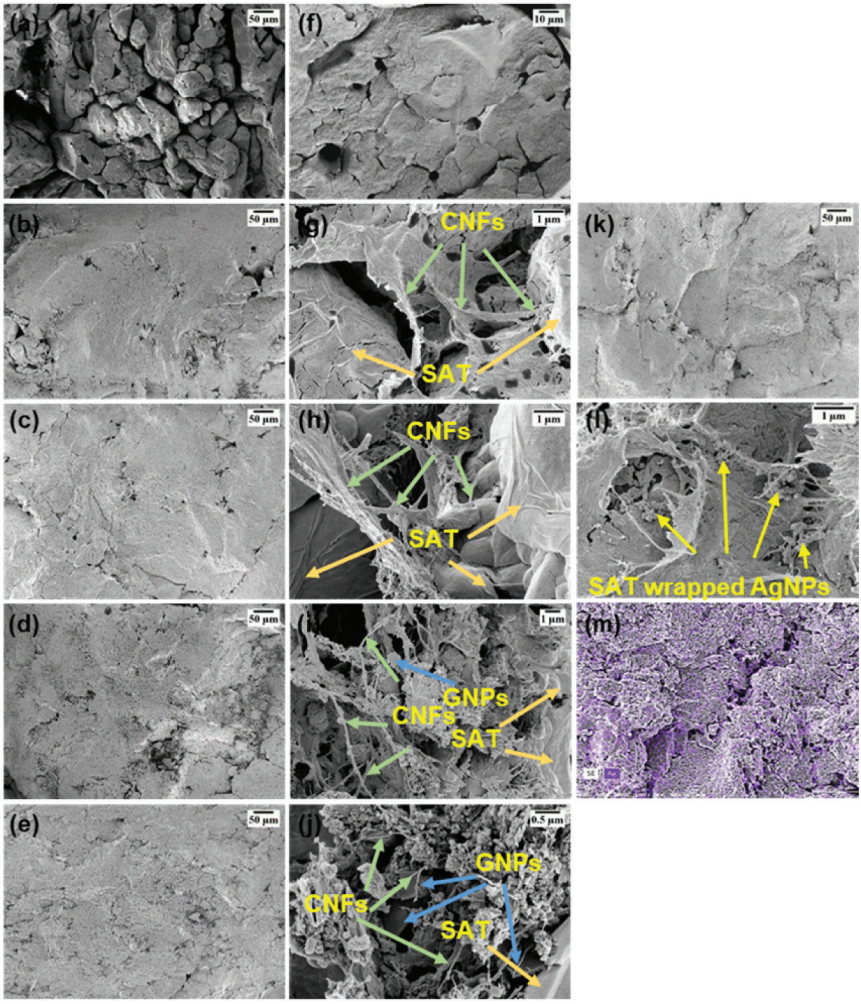

Figure 11. Low magnification SEM images of (a) SAT, (b) PCM@CNFs, (c) PCM@CNFs/$GNPs_{0.5}$, (d) PCM@CNFs/$GNPs_{1.5}$, (e) PCM@CNFs/$GNPs_{2.5}$, (k) PCM@CNFs/$AgNPs_{0.02}$; high magnification SEM images of (f) SAT, (g) PCM@CNFs, (h) PCM@CNFs/$GNPs_{0.5}$, (i) PCM@CNFs/$GNPs_{1.5}$, (j) PCM@CNFs/$GNPs_{2.5}$, (l) PCM@CNFs/$AgNPs_{0.02}$; (m) distribution of AgNPs in PCM@CNFs/$AgNPs_{0.02}$.

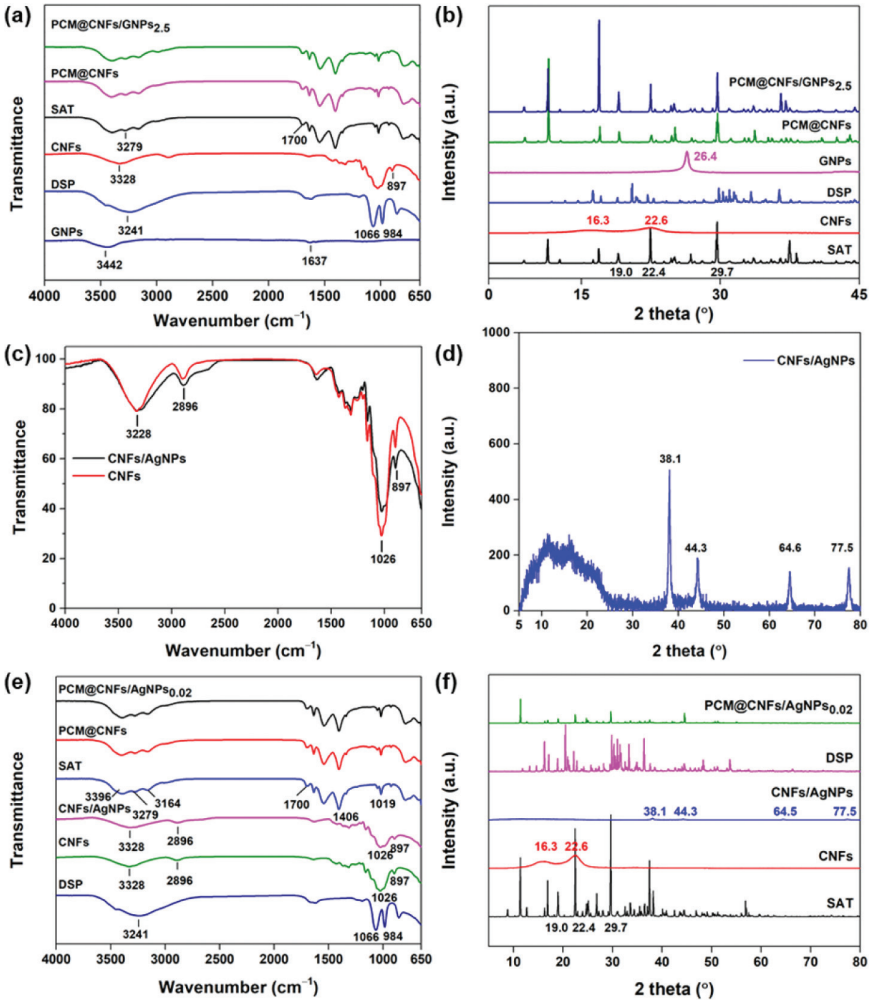

Figure 12. FT-IR spectra of (a) PCM@CNFs/$GNPs_{2.5}$ and its components, (c) CNFs and CNFs/$AgNPs_{0.02}$ composite and (e) PCM@CNFs/$AgNPs_{0.02}$ and its components; XRD patterns of (b) PCM@CNFs/$GNPs_{2.5}$ and its components, (d) CNFs/$AgNPs_{0.02}$ composite and (f) PCM@CNFs/$AgNPs_{0.02}$ and its components.

peaks between 3000 cm^{-1} and 3700 cm^{-1} due to the antisymmetric stretching vibration of –OH groups of crystal water [25] and peak at 1700 cm^{-1} due to the stretching vibration of C=O bond of carboxyl salt [26], are visible. The typical peak of hydroxyl groups at 3328 cm^{-1} and glucosidic linkages of cellulose at 897 cm^{-1} [27] can be found. In the spectrum of DSP, the peak at 3241 cm^{-1} is ascribed to crystal water, and peaks at 1066 cm^{-1} and 984 cm^{-1} are ascribed to P–O stretching and PO–H bending, respectively. In the spectrum of GNPs, the two peaks at 3442 cm^{-1} and 1637 cm^{-1} are assigned to O–H stretching and C=C bending vibrations [28], respectively. The spectrum of CNFs is compared with that of CNFs/$AgNPs_{0.02}$ composite (Figure 12(c)), and the widening of –OH groups at 3228 cm^{-1} and decrease of peak intensities at 2896 cm^{-1}, 1026 cm^{-1} and 897 cm^{-1} verify the successful synthesis of CNFs/AgNPs composite [29]. The XRD pattern of CNFs/AgNPs composite (Figure 12(d)) also displays the characteristic (1 1 1), (2 0 0), (2 2 0) and (3 1 1) crystal planes of AgNPs at 38.1°, 44.3°, 64.6° and 77.5° [30], respectively. As noted, the FT-IR spectra of composite PCMs are simply the mixture of all the characteristic peaks of each component and no new peaks are generated, i.e. no chemical reactions occurred in the preparation of composite PCMs. The results of XRD analysis (Figure 12(b) and Figure 12(f)) support this finding.

3.5 Phase Change Properties of Composite PCMs

The phase change properties of PCM samples, including melting point and enthalpy were determined by DSC analysis. The obtained DSC curves are presented in Figure 13 and the calculated melting point and enthalpy of samples are summarized in Table 2. The melting point and enthalpy determined here are slightly different from the most reported values of 264 kJ/kg and 58 °C, which is possibly due to the small sample amount (< 50 mg) used for DSC analysis. It is noted that both the melting point and enthalpy of the PCM samples decreased compared to those of pure SAT. As no chemical reactions occurred between SAT and other components, the decrease in enthalpy is due to the decreased SAT proportion in composite PCM with the introduction of other components. The decrease in melting point is ascribed to the enhanced heat transfer by GNPs or AgNPs, which make the composite PCM absorb more heat within the same time and thus accelerate their phase change. Consequently, the melting of composite PCMs occurred earlier and led to decreased melting points, as also reported elsewhere [31]. The enthalpies of PCM@CNFs and PCM@CNFs/AgNPs remained the same although the dosage of CNFs/AgNPs (1.0%) was higher than CNFs (0.8%). In short, the prepared composite PCMs exhibited reasonable phase change properties, which make them promising for actual applications.

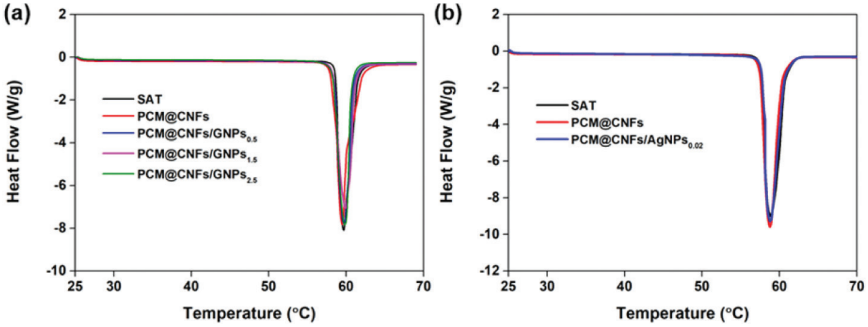

Figure 13. DSC curves of (a) SAT, PCM@CNFs and PCM@CNFs/GNPs composites and (b) SAT, PCM@CNFs and PCM@CNFs/$AgNPs_{0.02}$ composites.

Table 2. Melting points and enthalpies of the prepared PCM samples

PCM sample	*Melting point* (°C)	*Enthalpy* (kJ/kg)
SAT	58.7	270
PCM@CNFs	58.5	269
PCM@CNFs/$GNPs_{0.5}$	58.5	264
PCM@CNFs/$GNPs_{1.5}$	58.3	257
PCM@CNFs/$GNPs_{2.5}$	58.2	255
PCM@CNFs/$AgNPs_{0.02}$	57.4	269

3.6 Thermal Stability and Thermal Conductivity of Composite PCMs

The thermal stability of the prepared composite PCMs are examined by thermogravimetric analysis and the obtained TGA curves are presented in Figure 14. In the heating process of SAT, the free water in these samples evaporated first, and the bonds between anhydrous salt and its crystal water started to break when the temperature reached the melting point of PCM. The unbonded crystal water evaporated when the temperature continued to rise. When the temperature reached 138 °C, almost all moisture in SAT evaporated, and the residual weight fraction (60.03%) was almost identical to the theoretical solid content of pure SAT (60.28%). For composite PCMs, all their moisture evaporated at higher temperature, i.e. 150 °C for PCM@CNFs, 153 °C for PCM@CNFs/$GNPs_{2.5}$ and 160 °C for PCM@CNFs/$AgNPs_{0.02}$, suggesting their stronger water-holding ability and greater thermal stability over pure SAT. One thing to clarify is that CNFs with a pyrolysis temperature of 315–400 °C [32], GNPs with excellent stability at temperature over 800 °C [33] and silver nanoparticles with a melting temperature of 962 °C [34] were stable at such testing temperature, and they contributed to

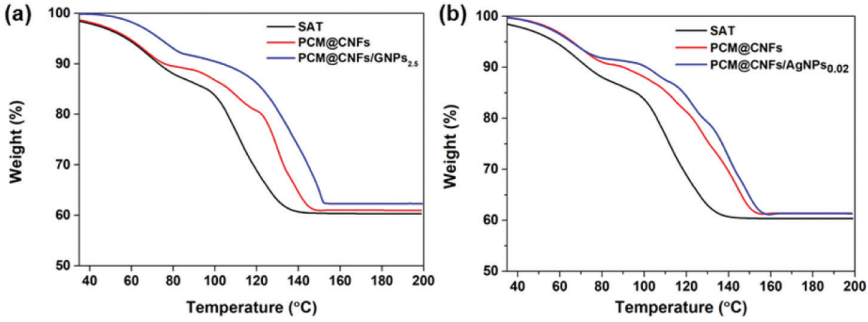

Figure 14. TGA curves of (a) SAT, PCM@CNFs and PCM@CNFs/$GNPs_{2.5}$ composites and (b) SAT, PCM@CNFs and PCM@CNFs/$AgNPs_{0.02}$ composites.

little weight loss of the tested composite PCMs. The hydrogen bond between CNFs and the crystal water of SAT and the introduction of thermally stable GNPs and AgNPs together contributed to the enhanced thermal stability. As noted, the residual weight fraction of composite PCM is above that of SAT, which can be ascribed to the incorporation of more solid components to PCM. In short, the prepared composite PCMs exhibited greater water-holding capability and enhanced thermal stability over SAT, benefiting their practical applications.

The thermal conductivity of PCMs is vital to heat transfer rate and the utilization efficiency of stored energy. Laser flash method that was suitable for measuring the thermal conductivity of salt hydrate PCMs [35] was adopted, and the results are shown in Figure 15. The measured thermal conductivity of pure SAT was 0.442 W/(m·K), quite similar to the value (0.433 W/(m·K)) reported elsewhere [36]. As seen in Figure 15(a), when increasing the proportion of GNPs in composite PCMs, the thermal conductivity enhanced accordingly, which is due to the excellent heat conduction performance of GNPs that act as the thermal channels in composite PCMs. When 2.5% of GNPs was applied, the thermal conductivity of PCM@CNFs/$GNPs_{2.5}$ reached 0.686 W/(m·K), which is 55.2% higher than that of pure SAT. Similar findings are discovered in Figure 15(b), i.e. increased addition levels of thermal conductivity enhancer (AgNPs) resulted in gradually improved thermal conductivity. When 1% of CNFs/$AgNPs_{0.02}$ composite was used, the thermal conductivity of composite PCM@CNFs/$AgNPs_{0.02}$ reached 0.58 W/(m·K), an improvement of 31.6% over that of pure SAT. Besides carbon nanomaterials, metal nanoparticles are also widely used as thermal conductivity enhancers. It can be expected that continuously increasing the addition level of carbon or metal nanoparticles results in further boosted thermal conductivity of composite PCMs, however, the accompanied possibility of easy aggregation of nanoparticles and the elevated cost should be weighed.

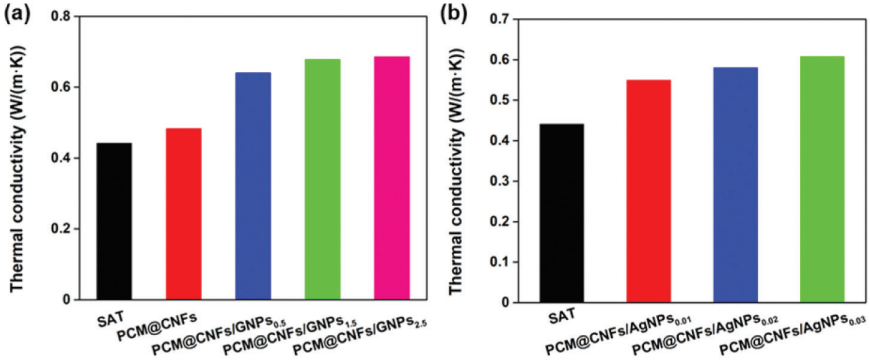

Figure 15. Thermal conductivity of (a) SAT, PCM@CNFs and composite PCMs containing GNPs and (b) SAT and composite PCMs containing AgNPs.

Moreover, both the type and dose of thermal conductivity enhancers influence their efficiency in improving the heat transfer performance of prepared composites, and this should be cared for in research.

3.7 Thermal Reliability of Composite PCMs

Thermal reliability is essential to the functioning reliability of a PCM-based TES system and its life span. The results of thermal reliability measurements are presented in Figure 16. Figure 16(a) and Figure 16(c) compare the FT-IR spectra of PCM@CNFs/$GNPs_{2.5}$ and PCM@CNFs/$AgNPs_{0.02}$ before and after 100 melting/freezing cycles, respectively. Comparison of FT-IR spectra suggests that the main peaks of the composite PCMs did not diminish or shift after the cyclic thermal tests and no new peaks were generated, suggesting the chemical stability of the composites. Again, the results confirmed the absence of chemical reaction between PCM and other components in repeated phase transitions. The melting point and phase change enthalpy of composite PCMs after 100 thermal cycles were obtained from their DSC curves (Figure 16(b) and Figure 16(d)) and are tabulated in Table 3. After the repeated melting/freezing cycles, the melting point of PCM@CNFs/$GNPs_{2.5}$ decreased slightly to 57.9 °C, and the enthalpy was 229 kJ/kg, decreased by 10.2%. Although the thermal reliability of this composite PCM is comparable with other reports [37,38], it needs to be improved for more endurable and reliable applications. The melting point of PCM@CNFs/AgNPs remained constant during the cyclic melting and freezing, and the enthalpy decreased by 2.2%, showing satisfactory thermal reliability for long term applications.

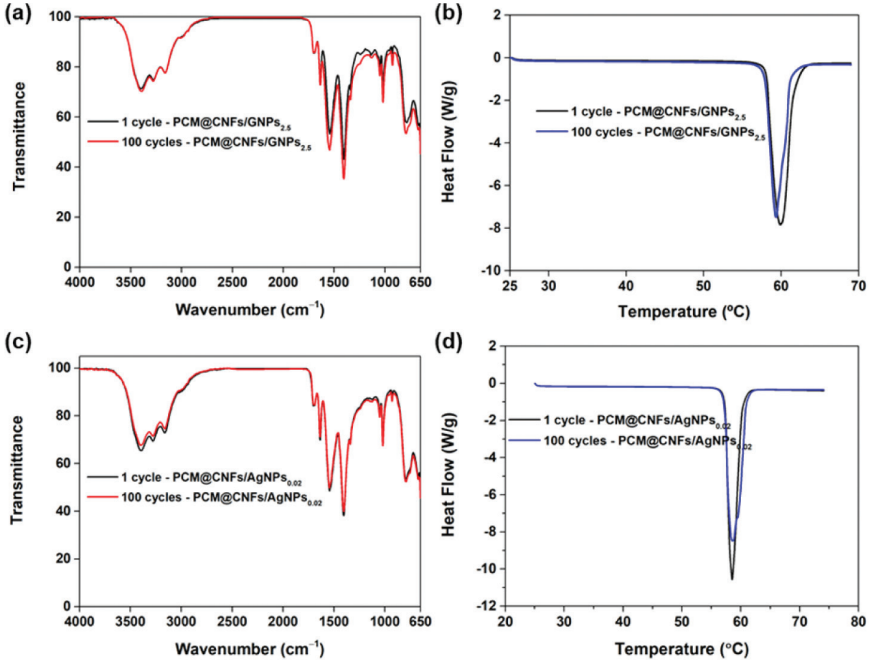

Figure 16. Thermal reliability tests: FT-IR spectra of (a) PCM@CNFs/GNPs$_{2.5}$ and (c) PCM@CNFs/AgNPs$_{0.02}$ before and after 100 melting/freezing cycles; DSC curves of (b) PCM@CNFs/GNPs$_{2.5}$ and (d) PCM@CNFs/AgNPs$_{0.02}$ before and after 100 melting/freezing cycles.

Table 3. Melting points and enthalpies of PCM samples measured before and after 100 melting/freezing cycles

PCM sample	*Melting point* (°C)	*Enthalpy* (kJ/kg)
PCM@CNFs/GNPs$_{2.5}$ (1 cycle)	58.2	255
PCM@CNFs/GNPs$_{2.5}$ (100 cycles)	57.9	229
PCM@CNFs/AgNPs$_{0.02}$ (1 cycle)	57.4	269
PCM@CNFs/AgNPs$_{0.02}$ (100 cycles)	57.4	263

4. CONCLUSIONS

In this work, CNFs/GNPs and CNFs/AgNPs composites were prepared and used to overcome the disadvantages of salt hydrate PCMs for efficient TES applications. The prepared cellulose nanofibrils/salt hydrate composite PCMs did not suffer from phase separation as the entangled CNFs networks and increased

viscosity contributed to the phase stability. Because of the excellent dispersing and stabilizing capability of CNFs, the aggregation of carbon nanomaterials and silver nanoparticles were avoided. Due to the compatibility of CNFs-based composites with other components, the prepared composite PCMs exhibited compact structures and improved thermal stability. Moreover, the use of CNFs/GNPs composite did not influence the supercooling suppression efficiency of DSP. The synergistic effect of DSP and CNFs/$AgNPs_{0.02}$ composite decreased the supercooling degree of SAT to 1.2 °C. Due to the presence of GNPs and AgNPs, the thermal conductivity of the corresponding composite PCM improved by 55.2% and 31.6% compared to that of pure SAT, respectively. Therefore, the prepared composite PCMs showed improved performances and have a greater potential for thermal energy storage applications.

REFERENCES

[1] J. Yan, D. Hu, Z. Wang and W. Ma. Construction strategies and thermal energy storage applications of shape-stabilized phase change materials. *J. Appl. Polym. Sci.* 139(4): e51550, 2022.

[2] M.M. Farid, A.M. Khudhair, S.A.K. Razack and S. Al-Hallaj. A review on phase change energy storage: Materials and applications. *Energy Convers. Manage.* 45(9–10): 1597–1615, 2004.

[3] G. Englmair, C. Moser, S. Furbo, M. Dannemand and J. Fan. Design and functionality of a segmented heat-storage prototype utilizing stable supercooling of sodium acetate trihydrate in a solar heating system. *Appl. Energy* 221: 522–534, 2018.

[4] M. Dannemand, J.M. Schultz, J.B. Johansen and S. Furbo. Long term thermal energy storage with stable supercooled sodium acetate trihydrate. *Appl. Therm. Eng.* 91: 671–678, 2015.

[5] Z. Zhang, Z. Duan, D. Chen, Y. Xie, X. Cao, and J. Wang. Sodium acetate trihydrate-based composite phase change material with enhanced thermal performance for energy storage. *J. Energy Storage* 34: 102186, 2021.

[6] M. Fashandi and S.N. Leung. Sodium acetate trihydrate-chitin nanowhisker nanocomposites with enhanced phase change performance for thermal energy storage. *Sol. Energy Mater. Sol. Cells* 178: 259–265, 2018.

[7] A. Safari, R. Saidur, F.A. Sulaiman, Y. Xu, and J. Dong. A review on supercooling of phase change materials in thermal energy storage systems. *Renew. Sust. Energ. Rev.* 70: 905–919, 2017.

[8] H. Lei, C. Fu, Y. Zou, S. Guo, and J. Huo. A thermal energy storage composite with sensing function and its thermal conductivity and thermal effusivity enhancement. *J. Mater. Chem. A* 7(12): 6720–6729, 2019.

[9] D. Klemm, B. Heublein, H.P. Fink, and A. Bohn. Cellulose: Fascinating biopolymer and sustainable raw material. *Angew. Chem. Int. Ed.* 44(22): 3358–3393, 2005.

[10] M. Pääkkö, M. Ankerfors, H. Kosonen, A. Nykänen, S. Ahola, M. Österberg, J. Ruokolainen, J. Laine, P.T. Larsson, and O. Ikkala. Enzymatic hydrolysis combined with mechanical shearing and high-pressure homogenization for nanoscale cellulose fibrils and strong gels. *Biomacromolecules* 8(6): 1934–1941, 2007.

[11] O. Nechyporchuk, M.N. Belgacem, and F. Pignon. Rheological properties of micro-/nanofibrillated cellulose suspensions: Wall-slip and shear banding phenomena. *Carbohydr. Polym.* 112: 432–439, 2014.

[12] M. Kaushik and A. Moores. Review: Nanocelluloses as versatile supports for metal nanoparticles and their applications in catalysis. *Green Chem.* 18(3): 622–637, 2016.

[13] Y. Li, H. Zhu, F. Shen, J. Wan, S. Lacey, Z. Fang, H. Dai, and L. Hu. Nanocellulose as green dispersant for two-dimensional energy materials. *Nano Energy* 13: 346–354, 2015.

[14] Y. Zhang, Y. Jiang and Y. Jiang. A simple method, the history method, of determining the heat of fusion, specific heat and thermal conductivity of phase-change materials. *Meas. Sci. Technol.* 10(3): 201, 1999.

[15] W. Hua, X. Zhang, M.J. Muthoka, and X. Han. Preparation and performance analysis of modified sodium acetate trihydrate. *Materials* 11(6): 1016, 2018.

[16] W. Kong, M. Dannemand, J. Brinkø Berg, J. Fan, G. Englmair, J. Dragsted, and S. Furbo. Experimental investigations on phase separation for different heights of sodium acetate water mixtures under different conditions. *Appl. Therm. Eng.* 148: 796–805, 2019.

[17] J. Liu, C. Zhu, W. Liang, Y. Li, H. Bai, Q. Guo, and C. Wang. Experimental investigation on micro-scale phase change material based on sodium acetate trihydrate for thermal storage. *Sol. Energy* 193: 413–421, 2019.

[18] Y. Wang, K. Yu, H. Peng, and X. Ling. Preparation and thermal properties of sodium acetate trihydrate as a novel phase change material for energy storage. *Energy* 167: 269–274, 2019.

[19] K. Oh, S. Kwon, W. Xu, X. Wang, and M. Toivakka. Effect of micro- and nanofibrillated cellulose on the phase stability of sodium sulfate decahydrate based phase change material. *Cellulose* 27(9): 5003–5016, 2020.

[20] D.C. Pozzo, K.R. Hollabaugh, and L.M. Walker. Rheology and phase behavior of copolymer-templated nanocomposite materials. *J. Rheol.* 49(3): 759–782, 2005.

[21] J. Polte, X. Tuaev, M. Wuithschick, A. Fischer, A.F. Thuenemann, K. Rademann, R. Kraehnert, and F. Emmerling. Formation mechanism of colloidal silver nanoparticles: Analogies and differences to the growth of gold nanoparticles. *ACS Nano* 6(7): 5791–5802, 2012.

[22] Q. Xu, L. Jin, Y. Wang, H. Chen, and M. Qin. Synthesis of silver nanoparticles using dialdehyde cellulose nanocrystal as a multi-functional agent and application to antibacterial paper. *Cellulose* 26(2): 1309–1321, 2019.

[23] J. Mao, J. Li, J. Li, G. Peng, and J. Li, *A selection and optimization experimental study of additives to thermal energy storage material sodium acetate trihydrate*. In *2009 International Conference on Energy and Environment Technology*, pp. 14–17, Guilin, China. IEEE Computer Society, Washington, 2009.

[24] J.J. De Yoreo and P.G. Vekilov. Principles of crystal nucleation and growth. *Rev. Mineral. Geochem.* 54(1): 57–93, 2003.

[25] T.A. Saleh. Simultaneous adsorptive desulfurization of diesel fuel over bimetallic nanoparticles loaded on activated carbon. *J. Clean. Prod.* 172: 2123–2132, 2018.
[26] C. Iacovita, R. Stiufiuc, T. Radu, A. Florea, G. Stiufiuc, A. Dutu, S. Mican, R. Tetean, and C.M. Lucaciu. Polyethylene glycol-mediated synthesis of cubic iron oxide nanoparticles with high heating power. *Nanoscale Res. Lett.* 10(1): 391, 2015.
[27] D.A. Gopakumar, A.R. Pai, Y.B. Pottathara, D. Pasquini, L. Carlos de Morais, M. Luke, N. Kalarikkal, Y. Grohens, and S. Thomas. Cellulose nanofiber-based polyaniline flexible papers as sustainable microwave absorbers in the X-band. *ACS Appl. Mater. Interfaces* 10(23): 20032–20043, 2018.
[28] N. Kumar and V.C. Srivastava. Simple synthesis of large graphene oxide sheets via electrochemical method coupled with oxidation process. *ACS Omega* 3(8): 10233–10242, 2018.
[29] G.-J. Kwon, S.-Y. Han, C.-W. Park, J.-S. Park, E.-A. Lee, N.-H. Kim, M. Alle, R. Bandi, and S.-H. Lee. Adsorption characteristics of Ag nanoparticles on cellulose nanofibrils with different chemical compositions. *Polymers* 12(1): 164, 2020.
[30] I. Ali, M.R. Akl, G.A. Meligi, and T.A. Saleh. Silver nanoparticles embedded in polystyrene-polyvinyl pyrrolidone nanocomposites using γ-ray irradiation: Physicochemical properties. *Results Phys.* 7: 1319–1328, 2017.
[31] T. Qian, J. Li, W. Feng, and H.e. Nian. Enhanced thermal conductivity of form-stable phase change composite with single-walled carbon nanotubes for thermal energy storage. *Sci. Rep.* 7(1): 1–10, 2017.
[32] H. Yang, R. Yan, H. Chen, D.H. Lee, and C. Zheng. Characteristics of hemicellulose, cellulose and lignin pyrolysis. *Fuel* 86(12–13): 1781–1788, 2007.
[33] K. Kim, W. Regan, B. Geng, B. Alemán, B.M. Kessler, F. Wang, M.F. Crommie, and A. Zettl. High-temperature stability of suspended single-layer graphene. *Phys. Status Solidi – Rapid Res. Lett.* 4(11): 302–304, 2010.
[34] M.M. Menamparambath, C.M. Ajmal, K.H. Kim, D. Yang, J. Roh, H.C. Park, C. Kwak, J.Y. Choi, and S. Baik. Silver nanowires decorated with silver nanoparticles for low-haze flexible transparent conductive films. *Sci. Rep.* 5: 16371, 2015.
[35] F. Kleiner, K. Posern, and A. Osburg. Thermal conductivity of selected salt hydrates for thermochemical solar heat storage applications measured by the light flash method. *Appl. Therm. Eng.* 113: 1189–1193, 2017.
[36] J.B. Johansen, M. Dannemand, W. Kong, J. Fan, J. Dragsted, and S. Furbo. Thermal conductivity enhancement of sodium acetate trihydrate by adding graphite powder and the effect on stability of supercooling. *Energy Procedia* 70: 249–256, 2015.
[37] J. Mao, P. Hou, R. Liu, F. Chen, and X. Dong. Preparation and thermal properties of SAT-CMC-DSP/EG composite as phase change material. *Appl. Therm. Eng.* 119: 585–592, 2017.
[38] Q. Xiao, J. Fan, L. Li, T. Xu, and W. Yuan. Solar thermal energy storage based on sodium acetate trihydrate phase change hydrogels with excellent light-to-thermal conversion performance. *Energy* 165: 1240–1247, 2018.

PREPARATION OF CELLULOSE NANOFIBRILS/SALT HYDRATE COMPOSITE PHASE CHANGE MATERIALS FOR THERMAL ENERGY STORAGE

Zhenghui Shen[1,2], *Kyudeok Oh*[3,4], *Martti Toivakka*[4], *Hak Lae Lee*[2,3]

[1] Beijing Key Laboratory for Theory and Technology of Advanced Battery Materials, School of Materials Science and Engineering, Peking University, Beijing 100871, China
[2] Department of Agriculture, Forestry and Bioresources, College of Agriculture and Life Sciences, Seoul National University, Seoul 08826, Korea
[3] Research Institute of Agriculture and Life Sciences, Seoul National University, Seoul 08826, Korea
[4] Laboratory of Natural Materials Technology, Åbo Akademi University, Turku 20500, Finland

Jon Phipps FiberLean Technologies Ltd

I have an observation and a question. The observation concerns the dips in the viscosity versus shear rate profiles between 1 and 10 s^{-1}, which I think everyone who measures MFC suspensions in this way observes. I understand that it is caused by the fibrils rolling up into flocs or balls, which releases water and thus reduces the viscosity. The question is about alternatives to CNF that you might consider. There must be many polymeric suspension aids that in principle you could use. A lot of them would not work in a system with such a high salt content as yours, but there are probably a fair few that would. Is there something special about the use of cellulose nanofibrils to suspend the particles that makes them better than any of the alternatives?

Discussion

Hak Lae Lee

There are many people who have tried to use synthetic polymers or soluble polymers as components for latent heat thermal storage systems. As I have shown, they do work. In this research, we tried to use a more environmentally friendly polymeric material, which is CNFs, of course, as a substitute for synthetic polymers. The unique property of CNF to form a network structure with resistance to strong salt solutions has been found to be very advantageous as a component for thermal energy storage applications. In particular, the network structure of CNF that does not change in a highly salty environment, which prevents small salt anhydride particles from settling down to the bottom and keeping them in place. It is noteworthy that highly charged CMC and TEMPO-oxidised CNF suspensions lose their structure in the highly salty condition.

Alexander Bismarck University of Vienna

I do not understand the problem of supercooling. If you have 60 or 58˚C, the material starts melting. Would not it be beneficial if I released the latent heat only at a temperature required?

Hak Lae Lee

When trying to increase the temperature of a thermal energy storage system, supercooling is not a problem. From a practical point of view, we usually want to raise the temperature of a phase change material above its freezing point and recover the stored energy when it cools below its freezing point. Supercooling of a material occurs when the temperature of the phase change material decreases lower than its melting point without crystallisation. In this case, the phase change material does not release the latent heat that we want to retrieve. In this case, the system acts like a simple sensible heat storage system rather than a latent heat storage system.

Alexander Bismarck

Okay, I lose heat because I heat all the supercooled solution again. But latent heat is latent heat, and it is still released, even if supercooled.

Hak Lae Lee

Yes, it releases some heat when supercooled. However, since latent heat is only released when it crystallises, the amount of heat released is much less. In other words, only sensible heat is released, and no latent heat unless it crystallises.

Robert Pelton McMaster University

Could you disperse these materials in a very open filter paper? Could you just saturate a filter paper? For the whole system, could you use a very porous network, instead of having a bulk material? What if it was dispersed in a fibre matrix? Would it solve some of the sedimentation problems?

Hak Lae Lee

The thing is that the amount of stored thermal energy is proportional to the amount of the phase change material in the system. If we want have a larger heat storage system, it is necessary to have a large storage tank filled with the phase change material.

Robert Pelton

I'm always looking for new uses for paper.